JOURNAL OF CATALYSIS 139, 392–405 (1993)

Acetonitrile Synthesis from CO, H_2, and NH_3 over Iron Catalysts

A. A. HUMMEL, M. V. BADANI, K. E. HUMMEL, AND W. N. DELGASS[1]

School of Chemical Engineering, Purdue University, West Lafayette, Indiana 47907-1283

Received May 21, 1992; revised September 8, 1992

The reaction of 1:2:1 $CO:H_2:NH_3$ at 698–723 K over reduced or prenitrided iron powder is initially active for production of CH_3CN, but deactivates quickly due to extensive carbon deposition. Much longer periods of stability are observed over a highly dispersed, prereduced Fe/SiO_2 or Fe on carbon catalysts, suggesting the importance of small particle size for resistance to coking. Prereduced Fe/SiO_2 catalysts containing only Fe^{2+} are less active for the nitrile reaction initially than those containing larger particle Fe^0 or Fe_2N phases, but increase in activity with time on stream. Mössbauer spectroscopy measurements indicate that the nitrided Fe/SiO_2 catalyst is converted in minutes to Fe carbide during reaction. Thus little or no bulk nitrogen remains during reaction. Fe^0 in supported or unsupported catalysts quickly converts to a carbide during reaction as well. Unlike the unsupported catalyst, which ceases to be active, the supported catalyst always maintains some finite activity. This activity is attributed to the iron particles that are below the size that produces excessive carbon deposition.

INTRODUCTION

The addition of ammonia to synthesis gas is known to produce amines at high pressures (30–100 atm) and relatively low temperatures (473 K) (*1–5*) and nitriles at higher temperatures, as described in Monsanto patents (*6–8*) and work done separately by Hamada *et al.* (*9*) and Tatsumi *et al.* (*10*). The Monsanto work describes the use of CO, H_2, and NH_3 over either iron or promoted molybdenum catalysts to produce acetonitrile in the temperature range 620–820 K. Pretreating the catalysts by reduction, nitriding, or carburizing was noted. The catalysts were also reported to possess additional catalytic activity when used in conjunction with refractory catalyst supports. The reaction proceeds well at atmospheric pressure, and selectivity to acetonitrile was found to be enhanced by addition of CO_2 to the reaction mixture (*8*). This may be due to the inhibition of the water gas shift reaction. The presence of Mn, Sr, Ba, Ca, or Ag components added to the Mo catalyst improves selectivity to acetonitrile (*7, 9*).

We have investigated the nitrile synthesis over unsupported and supported iron catalysts at atmospheric pressure, using mass spectrometry and gas chromatography for kinetic measurements, and Mössbauer spectroscopy for characterization of the catalysts. The most stable catalysts were carbon-supported and uncalcined silica-supported catalysts. Reduction of the silica-supported catalysts at 673 K in hydrogen resulted in a material with most, if not all, of the iron stabilized in the Fe^{2+} state.

Iron nitrides have been reported as good precursors for catalysts for synthesis gas reactions (*11*), although the surface nitride is rapidly decomposed during reaction (*12*). The present study concludes that the bulk nitride is also decomposed quickly during reaction in CO, H_2, and NH_3 at 723 K and fails to enhance the long term activity compared to that of its reduced counterpart.

EXPERIMENTAL

Catalyst preparation. Five iron catalysts, one iron powder, three silica-supported, and one carbon-supported, were prepared for this study. The iron powder catalyst was prepared at 343 K by precipitation after ad-

[1] To whom correspondence should be addressed.

0021-9517/93 $5.00

dition of NH_4OH to a 0.17 *M* $Fe(NO_3)_3 \cdot 9H_2O$ solution in triply distilled water. The resulting filter cake was dried in ambient air for 2 days, then heated in air at 373 K for 24 hr and finally at 573 K for 4 hr. The surface area of this catalyst, after reduction in H_2 at 673 K, was measured by a flowing BET method (*13*) and found to be 1.4 m^2/g of Fe_2O_3 precursor.

The silica-supported catalysts, designated (A), (B), and (C), were prepared in separate batches by incipient wetness impregnation of a dried Cab-O-Sil EH-5 silica with an iron nitrate solution, forming 4% Fe/SiO_2 catalysts. These catalysts were dried for 1–2 weeks in air and then vacuum dried (decomposed) at 423 K, followed by final treatment in flowing H_2 at 573 K for several hours. The catalysts were cooled to room temperature in He and passivated in 1% O_2 in helium before exposure to air. This method of preparation (that is, without calcination in O_2 mixtures) generally yields supported catalysts that are difficult to reduce below the Fe^{2+} state in H_2 at 673 K (*14*). In spite of the similarity of preparation, the catalysts (A), (B), and (C) have slightly different initial dispersions, resulting in different amounts of Fe^0 and Fe^{2+} in the reduced state.

The carbon-supported catalyst was prepared using a high-purity, high-surface-area amorphous carbon black, CSX203, supplied by Cabot Corporation. As received, CSX203 has been reported to contain a sufficient level of sulfur impurity to render the subsequent iron catalysts inactive. A desulfurization treatment (*15*), involving heating the support for 12 hr at 1223 K in flowing H_2, reduced the sulfur content of the CSX203 from 6550 ppm to 1860 ppm, as determined by X-ray fluorescence. The resulting carbon black contains a wide distribution of pore sizes, including an abundance of micropores. The total surface area of the desulfurized support was 1310 m^2/g, measured by the flowing BET method using N_2. The desulfurized support was impregnated with aqueous iron nitrate solution, forming an 11.85% Fe/CSX203 catalyst. Care was taken not to exceed the incipient wetness point. The subsequent drying and passivating procedure was similar to that used for silica-supported catalysts. The total surface area of the decomposed catalyst was found to be 1120 m^2/g.

The 11.85% Fe/CSX203 catalyst was further characterized by hydrogen desorption, TEM and Mössbauer spectroscopy. Hydrogen desorption, which involves heating in flowing H_2/Ar mixtures to 673 K, cooling in that mixture, and then heating in flowing Ar and detecting the desorbed H_2 (*16*), revealed an average particle size of 33 Å for reduced iron, corresponding to a dispersion of 26%. TEM studies, done in Dr. N. Otsuka's Laboratory (*17*), showed iron oxide particles with an average size of 25 Å, consistent with the hydrogen chemisorption measurements of the reduced catalyst. The Mössbauer spectra of the reduced and nitrided catalysts are presented in the results section.

Before reaction, the catalyst sample was activated *in situ* by reducing or nitriding. The reduction pretreatment was carried out in flowing H_2 at 673 K. Fe/SiO_2 was reduced for 12 hr, while the Fe/CSX203 catalyst was reduced for 16 hr. The nitrided catalyst was prepared by treating the prereduced catalyst in flowing NH_3 at 673 K for 12 hr. After these treatments, the catalyst was taken to the reaction temperature in the pretreatment atmosphere (H_2 or NH_3). Once the reaction temperature was stabilized, the reaction was initiated by switching from the pretreatment gas to the reaction gas mixture.

Mössbauer spectroscopy. The Mössbauer cell in which the sample was mounted was made of 316 stainless steel and equipped with beryllium windows. In CO, H_2, and NH_3 mixtures at temperatures above 673 K, 316 stainless steel corrodes, causing "dusting" of the metal surface (*18*). Thus, *in situ* spectra of catalysts reacted in the CO, H_2, and NH_3 environment were limited to 15 min of reaction time. The gas-phase reaction mixture was swept away with helium as soon as the cell cooled to 573 K. Spectra

involving catalysts exposed to the reaction mixture for longer time periods in a separate reactor were obtained from samples in a holder in air, after passivation of the used catalysts in a 1% O_2 in He mixture.

The Mössbauer spectra were obtained with an Austin Science S-600 spectrometer controller and a Nuclear Data model 62 multichannel analyzer. The source was ^{57}Co-Rh and the isomer shift reference was a 25-μm NBS α-iron foil. Fitting of the Mössbauer spectra was accomplished using a Levenberg–Marquardt least-squares routine, developed in our laboratories by Gregg Howsmon (*19*). The program fits isomer shift, quadrupole splitting, hyperfine splitting, linewidth, and total absorbance for each distinct species, and includes optional constraints on those parameters. All six-line patterns shown in this study were made up of Lorentzian-shaped lines fixed at 3 : 2 : 1 : 1 : 2 : 3 absorption intensity ratios. The routine can also fit a distribution of hyperfine fields at a fixed isomer shift and quadrupole splitting (*20*). The fitting routine and other details concerning this apparatus have been described elsewhere (*12*).

Reaction. One kinetic apparatus analyzed products by gas chromatography; a second used mass spectrometry. In the first system, a Hewlett–Packard 5830A chromatograph was equipped with a Supelco Porapak Q column (8 ft) in series with Porapak R column (8 ft). The reaction was carried out in a U-tube, flow reactor immersed in a heated, fluidized sand bath. Typically 135 cc/min of reactants flowed over 100 mg of silica-supported catalyst or 40 mg of carbon-supported catalyst and the conversion was less than 1%. The second kinetic apparatus consisted of a quartz tube reactor within brass sheathing heated by a Research Incorporated IR oven and controlled by a Micristar temperature controller, with the thermocouple located between the quartz tube and brass sheathing. The reactor could be fed with gas from any of three manifolds. Products, or reactants passing through a reactor bypass, were analyzed by an Extrel Laboratories EMBA II modulated beam quadrupole mass spectrometer interfaced to a Digital Equipment Corporation MINC-11 minicomputer for data acquisition. The reactor bypass mode was used to carefully calibrate the mass spectrometer for each experiment. The mass spectrometer measured H_2O, HCN, and CO_2 most accurately, whereas the gas chromatograph was best for the acetonitrile and hydrocarbon products. Overlaps of fragments in the mass spectrometer prevented methane measurement there, while weak sensitivity to detection prevented HCN analysis in the gas chromatography.

The helium, argon, and hydrogen gases used were Matheson ultra-high-purity grade with Scott purifiers installed to further scavenge oxygen. CO (UHP Matheson) was filled directly from the production facility into aluminum cylinders to minimize iron carbonyl contamination of the reactant gas. NH_3 was Matheson research purity grade and used without further purification.

RESULTS

Kinetics. The stability of the reaction over the various catalysts employed is one of the central issues of this study. At the temperature of the reaction (673–723 K), certain iron catalysts displayed stable activity, avoiding extensive carbon poisoning that can easily occur in CO mixtures at these temperatures over iron catalysts (*21–24*). Figure 1 shows the approach to steady-state production of acetonitrile over reduced Fe/SiO_2 (A), reduced Fe/SiO_2 (B), and nitrided Fe/SiO_2 (B). Figure 2 shows the relatively steady production of acetonitrile, methane, and ethane plus ethylene over prereduced and prenitrided Fe/CSX203 catalysts. Due to the difficulty of determining the area of the active surface for the different catalysts used, the rates in Figs. 1 and 2 are normalized per gram of Fe in the catalyst sample. The conditions were virtually the same in all cases, namely, atmospheric pressure, 1 : 2 : 1 : 1 CO : H_2 : NH_3 : He at 698 K with the only difference being the type of catalyst used.

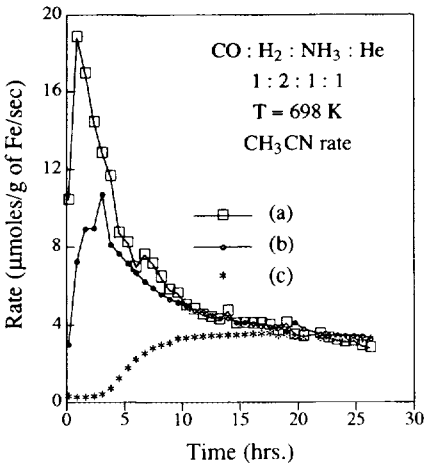

FIG. 1. Specific rate of synthesis of acetonitrile as a function of time on stream over (a) nitrided Fe/SiO_2 (B), (b) reduced Fe/SiO_2 (B), and (c) reduced Fe/SiO_2 (A).

The reactant ratio is close to the 2:7:3 $CO:H_2:NH_3$ ratio found by the Monsanto group to give maximum acetonitrile activity (*6–8*).

Although the catalysts in Fig. 1 were all prepared in similar fashion, the differences in the reaction behavior indicate that the nature of the iron in these prereduced or prenitrided samples is different. Nitriding an Fe catalyst has been shown to give a fast rise to high activity for the Fischer–Tropsch synthesis (*12, 25*), which is also the case here for nitrile production. One of the reduced catalysts also showed a rapid rise to high activity, while the other rose slowly to a steady state. Mössbauer results, discussed below, indicate that the catalysts that quickly achieve high activity contain relatively large particles of Fe^0 or Fe_2N before reaction, whereas the slowly activating catalyst has iron in the Fe^{2+} state before reaction.

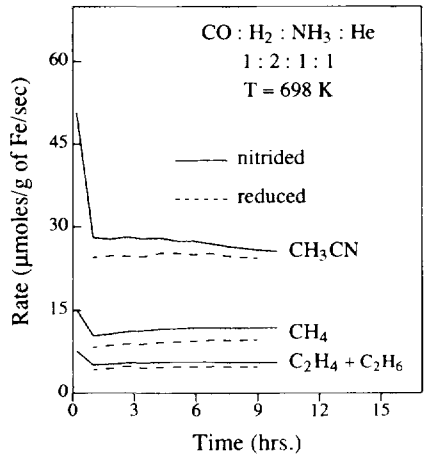

FIG. 2. Specific rate as a function of time for nitrided and reduced 11.85% Fe/CSX203 in 1:2:1:1 $CO:H_2:NH_3$:He at 698 K.

The active, stable carbon-supported catalyst, Fig. 2, establishes steady state much more quickly than the silica-supported materials. Stability of the Fischer–Tropsch reaction over iron catalysts supported on microporous or near microporous carbon has been shown before (*15, 26, 27*). Other examples exist, however, showing carbon-supported Fe catalysts that deactive during Fischer–Tropsch reaction (*21, 28–31*), indicating that the behavior of carbon-supported catalysts can be complex.

The acetonitrile synthesis reaction was also carried out at 723 K and atmospheric pressure over reduced iron powder by exposing the catalyst to 1:2:1 $CO:H_2:NH_3$. Unlike the supported catalysts, the reduced iron powder catalyst decays quickly and completely for all products in under an hour. In a separate experiment on Fe powder, the reaction stream was diluted with 66% He, but still showed the same rapid deactivation pattern. Thus, it is unlikely that deactivation is caused by a conversion-dependent temperature rise on the surface of the catalyst. That the complete deactivation of the unsupported Fe powder is due to the disproportionation (Boudouard) reaction, combined with the water–gas shift reaction, is shown by the fact that H_2O and CO_2 appeared as the major products:

$$2CO \rightarrow CO_2 + C(\text{solid}) \quad (1)$$

$$H_2 + CO_2 \rightarrow H_2O + CO. \quad (2)$$

The above reactions so dominate the surface

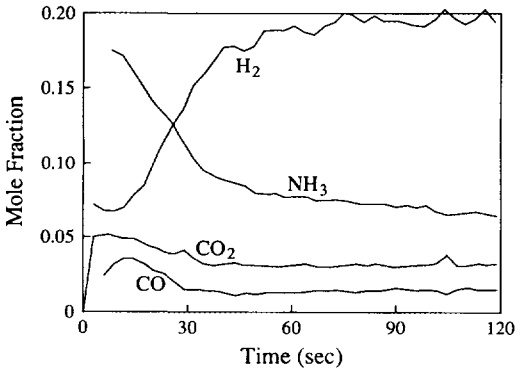

FIG. 3. Mass spectral analysis of a step change from NH_3 to 2:7:3 $CO:H_2:NH_3$ + 66% He over nitrided iron powder at 773 K.

reaction pathway over Fe powder that the catalyst deactivates quickly due to excessive carbon deposition. The carbon deposited from this reaction forms both bulk carbide and surface carbon, which blocks sites for other surface chemistry. The catalyst is nearly as active toward acetonitrile as supported iron initially, but the order of magnitude higher activity toward CO disproportionation quickly poisons the catalyst.

In contrast, as shown in Figs. 1 and 2, supported iron catalysts do not deactivate nearly so quickly. The reaction reaches an approximate steady state, in which oxygen in CO_2 and H_2O is approximately equal to the carbon in the nitriles with the difference made up by the conversion to hydrocarbons, as required by the synthesis stoichiometry in the absence of reaction (1). The above results lead to the unavoidable conclusion that there is a support or particle-size-induced effect on the coking rate.

The effect on the acetonitrile rate of bulk nitrogen introduced by prenitriding the catalyst was studied by transient experiments. Figure 3 shows the initial minutes of synthesis over the nitrided iron powder, as monitored with mass spectrometry. A sample of 240 mg of the iron powder catalyst was prereduced for 6 hr in H_2 at 723 K and prenitrided for 8 hr in NH_3 at 723 K before exposure to reaction conditions. The temperature was raised to 773 K in ammonia, then the catalyst was exposed at time zero to a 145 ml/min stream composed of 2:7:3 $CO:H_2:NH_3$ with 66% He added as a diluent. In NH_3 at 723 K, unsupported iron powder forms an ε/ζ-Fe_2N phase (*11*, *12*, *32*). In Fig. 3, the NH_3 curve drops to its steady-state value over the first minute of exposure, much more slowly than the fast rise in CO_2 production, characteristic of the rise time of the concentration step. Moreover, the lag in the H_2 curve indicates that the reaction

$$Fe_2N + 3/2\ H_2 \rightarrow NH_3 + 2\ Fe \qquad (3)$$

is occurring. The amount of "missing" hydrogen or "extra" ammonia, calculated from material balances on this experiment, correlates well with the complete conversion of Fe_2N to Fe by reaction (3). We may conclude, therefore, that the iron nitride decomposes during the first 30 sec under these conditions. Mössbauer results confirm complete decomposition of the nitride during reaction at 723 K for both iron powder and silica-supported iron catalysts. At lower temperatures in synthesis gas, prenitrided iron is known to form carbonitrides (*11*, *12*, *25*, *33*). While some retention of nitrogen in the carbides formed is possible at the higher temperatures of these studies, faster diffusion rates of nitrogen within the iron matrix provide for the removal of nearly all the nitrogen during nitride decomposition. Thereafter, the prenitrided iron powder catalyst behaves very much like its prereduced counterpart. The extensive carbon deposition, as evidenced by the high selectivity to CO_2 shown in Fig. 3, quickly poisons the activity.

Mössbauer spectroscopy. The kinetic results demonstrate radically different catalytic stability for the nitrile reaction over seemingly similar supported and unsupported prereduced or prenitrided iron catalysts. The different natures of these catalysts, namely, the oxidation state, nitride or carbide phase behavior, and clues about the

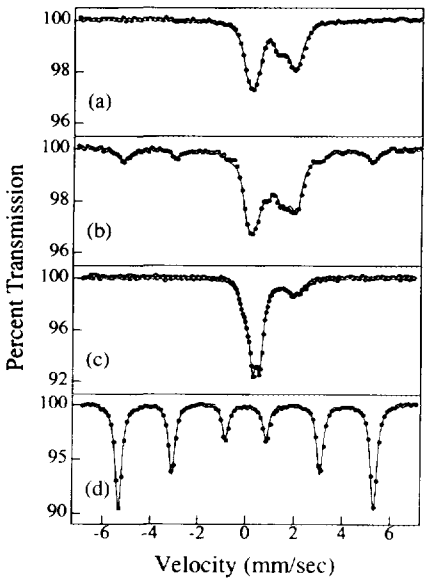

FIG. 4. Room-temperature Mössbauer spectra of (a) reduced Fe/SiO_2 (A), (b) reduced Fe/SiO_2 (B), (c) nitrided Fe/SiO_2 (B), and (d) reduced Fe powder catalysts.

particle size, can all be conveniently studied by Mössbauer spectroscopy.

Figure 4 shows the room temperature spectra of the reduced Fe/SiO_2 (A), reduced Fe/SiO_2 (B), nitrided Fe/SiO_2 (B), and reduced unsupported iron powder. The reduction pretreatment was for 12 hr, in H_2 at 673 K. For nitriding, the catalyst was further treated for 12 hr in NH_3 at 673 K. In all cases, the catalyst was cooled in the reducing or nitriding atmosphere to the room-temperature acquisition conditions. The reduced catalysts contain varying amounts of Fe^0, Fe^{2+}, and Fe^{3+}, while the nitrided catalyst is composed of Fe^{2+} and iron with two (Fe(2N)) and three (Fe(3N)) nearest nitrogen neighbors (*32*). As the nitride approaches the stoichiometry Fe_2N, all the iron has three nearest nitrogen neighbors and a complete transition to the orthorhombic ζ nitride occurs. Parameters for the fits are given in Table 1. The most striking result in Figure 4 is the difference between the spectrum of the reduced iron powder, which shows α-Fe, as expected from thermodynamics, and those of the reduced Fe/SiO_2 catalysts (Figs. 4a and 4b), which show large fractions of Fe that are irreducible beyond the Fe^{2+} state. Past studies of the effect of calcination and catalyst pretreatment on reducibility have shown that high-temperature pretreatment in an oxidizing atmosphere (i.e., calcination) sinters the iron phase and disengages iron particles from interacting strongly with the support (*14*). With the catalysts of Figs. 4a and 4b, however, the precursor decomposition occurred in an H_2 atmosphere at 573 K. Further reduction at 673 K does not nucleate a substantial amount of the Fe^0 phase.

By far the most abundant phase for the "irreducible" Fe/SiO_2 (A) sample is the higher coordination, larger IS and QS Fe^{2+}, which represents >70% of the spectral area. The low coordination, lower IS and QS Fe^{2+} is typically assigned to the surface species since iron atoms have incomplete coordination (*34*, *35*). The surface atoms have a smaller Debye temperature (*36*) and accompanying recoil free fraction, however, and their relative spectral area is smaller than the actual fraction of surface iron (*37*). The total Fe^{2+} abundance in the Fe/SiO_2 (A) catalyst approaches 100%. The Fe/SiO_2 (B) catalyst has the interesting characteristic of having both Fe^0 and Fe^{2+} components, with a total of 78% in the Fe^{2+} state, and 18% as Fe^0 iron, based on spectral area. The Fe^0 particles are small in this catalyst, as implied by the small field (323.3 kOe) for this phase (Table 1). As particle size decreases, the field decreases as a result of collective oscillations until it finally collapses to achieve superparamagnetism (*38*). The approximate relation between particle size and hyperfine field has been shown to be (*39*)

$$H_{obs} = H_0[1\text{-}kT/2KV], \qquad (4)$$

where H_{obs}, H_0 = observed and iron foil (330 kOe) hyperfine splittings, kT = thermal energy, K = magnetic anisotropy energy constant, and V = volume of particle.

The estimation of particle size using this

TABLE 1

Mössbauer Spectral Parameters for Fig. 4

Figure	Phase	IS (mm/sec)	QS (mm/sec)	HFS (kOe)	LW (mm/sec)	Rel. area (%)
4a	Fe^{2+}	1.05	1.84	—	0.71	72.7
	Fe^{2+} (low coord.)	0.79	1.02	—	0.50	23.2
	Fe^{3+}	0.21	0.58	—	0.20	4.1
4b	Fe^{0}	0.02	0.0	323.3	0.57	18.4
	Fe^{2+}	1.08	1.94	—	0.55	33.5
	Fe^{2+} (low coord.)	0.94	1.09	—	0.77	44.7
	Fe^{3+}	0.41	0.98	—	0.24	3.3
4c	Fe^{2+}	1.08	1.86	—	0.72	34.4
	Fe(3N)	0.42	0.28	—	0.31	46.7
	Fe(2N)	0.27	0.69	—	0.45	18.9
4d	Fe^{0}	0.0	0.0	331.7	0.33	100.0

method is only approximate, since the anisotropy energy constant is a function of many factors, including particle size and shape (*38*). Using the value of $K = 1.2 \times 10^5$ J/m^3 for 63 Å Fe particles on silica in H_2 at room temperature (*40*), we estimate the particle size of the magnetically split Fe^0 in Fe/SiO_2 (B) to be 95 Å. This reduced catalyst was initially active for the nitrile reaction at 698 K, reached a maximum activity, then decayed to a stable steady state (Fig. 1). Since the catalyst Fe/SiO_2 (A) that reduced only to Fe^{2+} in Fig. 1 rose slowly to a steady state activity, it appears that Fe° particles large enough to be magnetically split in the room-temperature Mössbauer system can lead quickly to a catalytically active surface, but cannot maintain that high activity.

The 11.85% Fe/CSX203 catalyst also started at a high activity. Figure 5 shows the room temperature Mössbauer spectra of the reduced and nitrided catalysts, with parameters listed in Table 2. The catalyst was reduced in H_2 for 16 hr at 673 K, spectrum 5a, followed by 6 hr of nitriding in NH_3 at 673 K, spectrum 5c. For the reduced catalyst, a significant fraction of the iron particles was small enough to display superparamagnetism. In this particle size range, the fit can be approximated by a distribution of magnetic fields, as shown in Fig. 5b. Spectrum 5a is fit with this distribution in addition to a magnetically split contribution with field of 325 kOe (noticeably smaller than the 330 kOe of bulk iron) and a small contribution

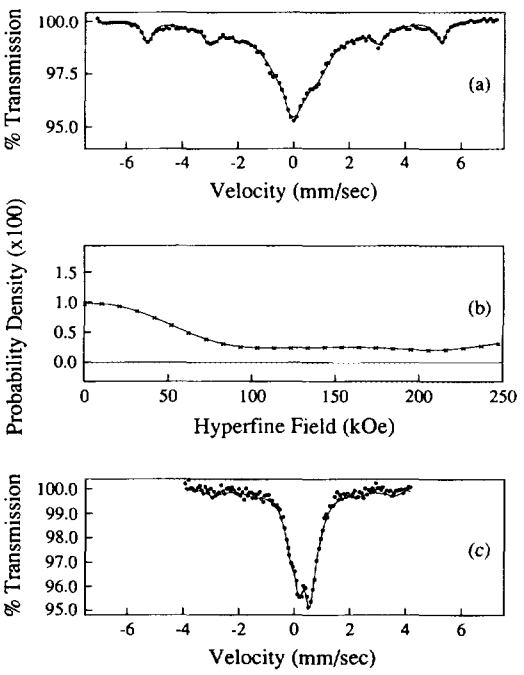

FIG. 5. Room-temperature Mössbauer spectra of (a) reduced and (c) nitrided 11.85% Fe/CSX203; (b) is the hyperfine field probability density function used in fitting spectrum (a).

TABLE 2

Mössbauer Spectral Parameters for Fig. 5

Figure	Phase	IS (mm/sec)	QS (mm/sec)	HFS (kOe)	LW (mm/sec)	Rel. area (%)
5a	Fe^{2+}	1.0	—	—	0.85	5.0
	Fe^0 (magnetic)	−0.01	0.0	325	0.47	19.4
	Fe^0 (dist.)	0.0	0.01	0–248	0.69	75.6
5c	Fe(3N)	0.41	0.35	—	0.35	32.7
	Fe(2N)	0.31	0.76	—	0.68	56.1
	Fe(2N)	0.34	−0.1	202	0.53	11.2

from an Fe^{2+} singlet, previously seen (*41*). Also highly active and stable is the nitrided Fe/CSX203 catalyst of Fig. 5c. This catalyst has spectral contributions from iron with two (Fe(2N)) and three (Fe(3N)) nitrogen nearest neighbor sites (*32*).

The phase structure of the silica-supported iron catalysts after reaction is shown by Mössbauer spectroscopy in Fig. 6, with parameters given in Table 3. Figure 6a is the room-temperature Mössbauer spectrum of Fe/SiO_2 (B) after it had been reduced for 12 hr at 673 K, as shown in Fig. 4b. When this catalyst was exposed *in situ* to 15 min of 1 : 2 : 1 CO : H_2 : NH_3 at 723 K, it gave spectrum 6b. Here, the fraction of α-Fe in Fig. 6a (18%) is approximately equal to the area of the carbide ε'-$Fe_{2.2}C$ with a magnetic splitting of 166.6 kOe.

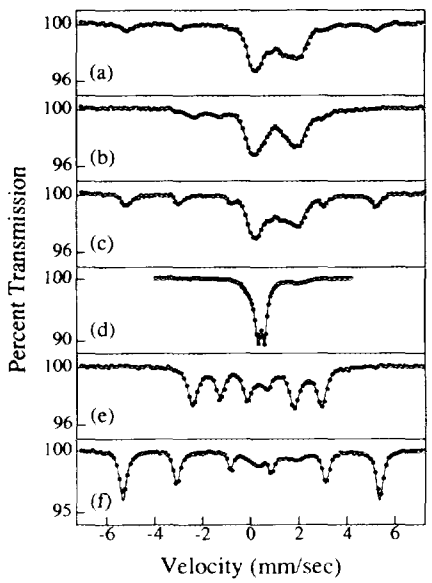

FIG. 6. Room temperature Mössbauer spectra of Fe/SiO_2 (B): (a) reduced; (b) 15 min of reaction after (a); (c) rereduced after (b); (d) nitrided after (c); (e) 15 min of reaction after (d); and (f) rereduced after (e).

Rereducing this catalyst in H_2 at 673 K for another 12 hr resulted in a catalyst with slightly greater area fraction of Fe^0 (27%), shown in Fig. 6c, as compared to the freshly reduced catalyst, Fig. 6a. These iron particles are still small, as indicated by the hyperfine field of 323.9 kOe. Apparently the Fe^0 fraction is carbided quickly during reaction,but can be returned to similar size Fe^0 particles by rereduction. The relative fraction of Fe^{2+} remains unchanged during the cycle of reduction/reaction/rereduction.

When the catalyst from spectrum 6c was treated with NH_3 at 673 K for 12 hr, only 18% of the area corresponding to Fe^{2+} remained (Fig. 6d). The spectrum also has contributions from iron nitrides with iron with two (Fe(2N)) and three (Fe(3N)) nitrogen nearest neighbor sites. After 15 min of reaction over this nitrided catalyst at 723 K, all of the nitride was converted to carbide, as shown in Fig. 6e. Once again, the Fe^{2+} fraction remains relatively unaffected. Consistent with nitride decomposition observed in Fig. 3 for the iron powder, little or no nitrogen remains in the bulk of the supported catalyst during reaction at these con-

TABLE 3

Mössbauer Spectral Parameters for Fig. 6

Figure	Phase	IS (mm/sec)	QS (mm/sec)	HFS (kOe)	LW (mm/sec)	Rel. area (%)
6a	Fe^0	0.02	0.0	323.3	0.57	18.4
	Fe^{2+}	1.08	1.94	—	0.55	33.5
	Fe^{2+} (low coord.)	0.94	1.09	—	0.77	44.7
	Fe^{3+}	0.41	0.98	—	0.24	3.3
6b	ε'-$Fe_{2.2}C$	0.21	0.05	166.6	0.59	21.4
	Fe^{2+}	1.06	1.94	—	0.62	42.5
	Fe^{2+} (low coord.)	0.93	1.16	—	0.72	31.2
	Fe^{3+}	0.29	0.84	—	0.27	4.9
6c	Fe^0	0.01	0.0	323.9	0.57	26.7
	Fe^{2+}	1.07	1.87	—	0.61	38.5
	Fe^{2+} (low coord.)	0.89	1.04	—	0.76	32.5
	Fe^{3+}	0.39	0.92	—	0.16	2.3
6d	Fe(3N)	0.43	0.28	—	0.24	56.1
	Fe(2N)	0.28	0.59	—	0.59	25.4
	Fe^{2+}	1.12	1.81	—	0.77	18.4
6e	ε'-$Fe_{2.2}C$	0.24	0.0	166.4	0.46	77.5
	Fe^{2+}	0.88	1.86	—	0.66	18.1
	Fe^{3+}	0.19	0.78	—	0.34	4.4
6f	Fe^0	0.00	0.00	332.8	0.36	80.3
	Fe^{2+}	1.15	1.72	—	0.51	8.3
	Fe^{2+} (low coord.)	0.84	1.39	—	0.72	9.4
	Fe^{3+}	0.31	0.97	—	0.72	2.0

ditions. This conclusion is drawn from the fact that the hyperfine field of 166.4 kOe for the carbide phase would have been much lower if nitrogen were incorporated.

Rereduction of the nitrided and reacted Fe/SiO_2 (B) sample in H_2 at 673 K for 12 hr converted all of the carbide to α-Fe, with a hyperfine field consistent with that of large particles (331.7 kOe), and the Fe^{2+} fraction remaining the same. This catalyst sintered during the cycle of nitriding/reaction/rereduction. Since the Fe^{2+} character was lost during the nitriding step, it is likely that sintering occurred in NH_3 during the nitriding procedure.

The steady state activity on the Fe/SiO_2 (B) catalyst after each step in the above cycle is shown in Fig. 7. The reactions were carried out at 723 K in 1 : 2 : 1 : 1 $CO : H_2 : NH_3 : He$. The activity behavior on reduced Fe/SiO_2 (B) is similar to that in Fig. 1, where the reaction was carried out at 698

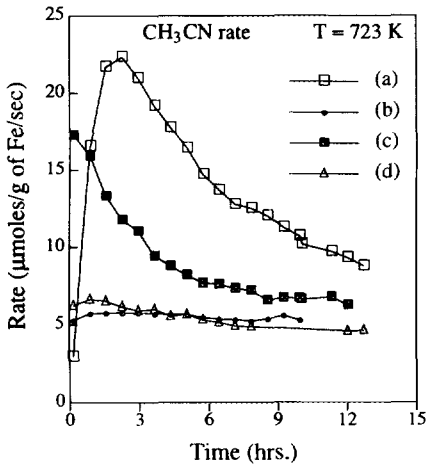

FIG. 7. Specific rate of acetonitrile production over Fe/SiO_2 (B) as a function of time: (a) reduced; (b) rereduced after (a); (c) rereduced and nitrided after (b); and (d) rereduced after (c).

K. In the present case, the reaction was carried out for 36 hr (although only the first 12 hr of activity is shown in Fig. 7). On the rereduced catalyst, the activity observed for 12 hr was very different from that of the freshly reduced material, showing no maximum. This is probably due to sintering during the preceding reaction cycle. Some sintering was confirmed by the high hyperfine field of α-Fe after rereduction, Fig. 6c, following only 15 min exposure to the reaction mixture. The absence of the maximum after rereduction indicates complete carburization of large particles within the first 10 min of reaction.

The initial activity and rapid decay of the nitrided catalyst corresponding to Fig. 6d is also different from that seen on a freshly nitrided catalyst (Fig. 1). Furthermore, the activity was much lower than that observed on freshly nitrided catalyst. This again points to severe sintering during the initial stages of the experiment. Further rereduction gives the same activity as that observed on the previous rereduced catalyst. This indicates that there was no more sintering during the later stages of rereduction/reaction/nitriding/reaction. The decrease in activity observed on the nitrided catalyst was only due to coking, as observed on large iron particles.

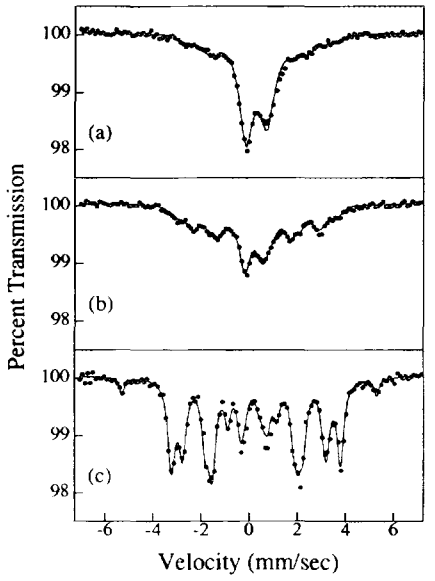

FIG. 8. Room-temperature Mössbauer spectra: (a) after 8 hr of reaction over reduced Fe/SiO_2 (C) and exposure to air; (b) after 24 hr of reaction over nitrided Fe/SiO_2 (C) and exposure to air; and (c) after 1 hr of reaction over reduced Fe powder.

The phases present after long-term exposure during the nitrile reaction are shown in the *ex situ* spectra of Fig. 8. Figure 8a shows the prereduced Fe/SiO_2 (C) catalyst after 8 hr of reaction at 723 K in 1 : 2 : 1 $CO : H_2 : NH_3$, and Fig. 8b is the spectrum of the prenitrided catalyst after 24 hr on-stream. The characteristics of reduced Fe/SiO_2 (C) catalyst are similar to those observed for Fe/SiO_2 (B). Since oxidation during air exposure degraded resolution by introducing additional overlapping iron phases, a distribtuion of magnetic fields was used to extract some relevant information from the spectra. Fits for both the spectra included a doublet for Fe^{3+}, a doublet for high coordination Fe^{2+} and a doublet for superparamagnetic (S.P.) carbide as well as the distribution. The parameters of the fits are listed in Table 4, while the distribution functions are shown in Fig. 9. From the distribution function we can see the presence of ε'-$Fe_{2.2}C$ (170–180 kOe) and χ-$Fe_{2.5}C$, which has three sets of sixline patterns (110–130, 170–185, and 210–220 kOe) (*42*). The unusually high amount of species with a field of 110–130 kOe may be due to presence of a carbonitride or some superparamagnetically relaxed carbide. The prereduced iron powder catalyst, completely inactive after an hour on stream, gave the spectrum shown in Fig. 8c, with parameters in Table 4. The phase formed is χ-$Fe_{2.5}C$ and a small fraction of the particle, presumably the center, which had not yet formed a carbide. The χ-carbide is also formed in preference to ε or ε' in large iron particles during the Fischer–Tropsch reaction (*43*).

DISCUSSION

The deposition of carbon on Fe plays the major role in determining the success or failure of these catalysts. Many types of carbon

TABLE 4

Mössbauer Spectral Parameters for Fig. 8

Figure	Phase	IS (mm/sec)	QS (mm/sec)	HFS (kOe)	LW (mm/sec)	Rel. area
8a	Fe^{3+}	0.3	0.9	—	0.6	47.0
	Fe^{2+}	1.08	2.1	—	0.7	10.7
	S.P. carbide	0.15	0.6	—	0.6	8.4
	Carbide (dist.)	0.18	0.28	75–235	0.46	33.9
8b	Fe^{3+}	0.32	0.96	—	0.6	13.7
	Fe^{2+}	1.12	2.17	—	0.7	3.3
	S.P. carbide	0.15	0.6	—	0.6	12.0
	Carbide (dist.)	0.21	0.07	75–235	0.46	71.0
8c	Fe^0	0.0	0.02	329.9	0.24	5.8
	χ-$Fe_{2.5}$(I)	0.18	0.04	186.2	0.36	35.4
	χ-$Fe_{2.5}$(II)	0.25	0.03	219.2	0.34	38.4
	χ-$Fe_{2.5}$(III)	0.2	0.08	110.2	0.32	20.3

are known to exist on an Fe surface in synthesis gas mixtures (*30, 44–48*). On bulk alumina- and silica-supported iron catalysts (44–47), bulk carbidic carbon, a surface carbidic carbon, an active surface carbon and surface graphite are known to form. Work with carbon-supported (*30*) and titania-supported (*48*) iron catalysts also showed similar kinetic behavior, but with differences in the rate of carburization and abundance of certain surface species. On Fe/ZnO, Kieffer and van der Baan (*23*) found evidence of multiple types of carbon on an iron surface that reconstructs during reaction. The abundance of graphitic carbon on iron surfaces during synthesis is a common theme of these and other studies (*21–24, 49*). The activity and irreversibility of graphitic carbon is the chief cause of deactivation (*50*).

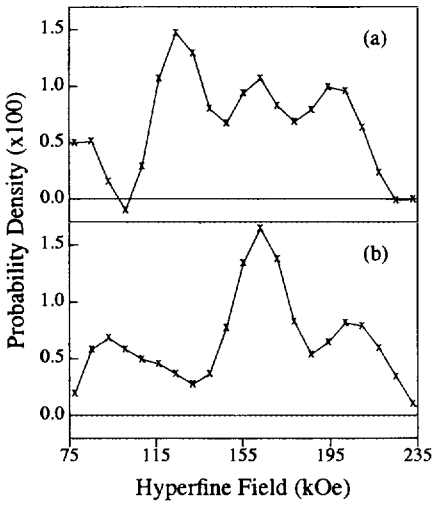

FIG. 9. Hyperfine field probability density functions used in fitting (a) spectrum 8a and (b) spectrum 8b.

In our experiments over freshly pretreated catalysts (i.e., no prior history of reaction), it appears that the lack of deactivation is observed only over small particles. This is implied by the stable activity observed over Fe/CSX203, where the particles are known to be small. Also, since ε'- and χ-carbide particles are formed slowly during the nitrile synthesis (Figs. 7 and 9), one may infer that the active and stable Fe/SiO_2 catalyst, originating from inactive Fe^{2+}, could be very small crystallites of iron carbide formed during reaction. The small particle tail of the size distribution may also account for stable activity over rereduced postreaction Fe/SiO_2 (B), where most of the catalyst is composed of large particles. The similarities in small particle behavior in silica- and carbon-supported catalysts suggests that particle size, rather than support interactions, plays the key role.

A particle-size effect for coking has been

well established in the literature for Pt (*50, 51*), Ni (*52, 53*), Ir (*54*) and Fe (*25*). Froment and Nam (*55*) have modeled deactivation due to site blockage using a stochastic dual-site mechanism, showing a theoretical dependence on ensemble size for deactivation. For Ni catalysts, such an effect was observed for steam reforming of hydrocarbons over 4–6 nm Ni/MgO catalysts (*52*) and for hydrogenolysis of several hydrocarbons over 1- and 6-nm Ni/Aerosil particles (*53*). In the latter study, the particle-size effect on poisoning offset an intrinsic particle-size dependence of the hydrogenolysis reaction. For synthesis gas conversion over Fe/MgO, however, McDonald and Boudart observed a particle-size effect for poisoning, but this was overwhelmed by the intrinsic effect for the synthesis of hydrocarbons (*25*). For Fe/CSX203 catalysts, Jung *et al.* also observed lower turnover frequencies for smaller particles (*26*).

In our results, the particle-size effect for the intrinsic reaction toward nitriles is difficult to assess, due to the rapid and total deactivation of the bulk iron powders at 723 K. However, the overall catalytic performance shows a particle-size effect, since nitrile production is stable over the high dispersion Fe/CSX203 catalysts. Furthermore, the initial nitrile production rates are similar for large and relatively small α-Fe particles. Thus, at high temperature and in the synthesis gas mixture including NH_3, the poisoning reaction is sensitive to particle size, which has more impact on the long-term nitrile or hydrocarbon activity than on initial activity.

The Fe/SiO_2 catalysts also showed stable activity when they were reducable only to the Fe^{2+} state before reaction. The irreducibility of the iron means that it is in close contact with the support, either as very small particles or in a raft-type structure. Other authors (*56–59*) have also observed stable synthesis gas activity over iron catalysts that are in an oxidic state before reaction. Venter *et al.* (*27*) have separated iron catalysts for synthesis gas into two groups, those that are highly dispersed Fe/C or, alternatively, poorly reduced catalysts, both of which display stable activity, and an another group of fully reducable unsupported or supported catalysts that deactivate during reaction. This distinction is supported by our results for the nitrile reaction. Results from Fig. 1 show, however, that the oxidic phase itself (in Fe/SiO_2 (A)) is not initially active for the nitrile reaction.

These data are all consistent with the conclusion that the nitrile reaction is primarily dependent on a particle-size effect on coking, and that the active phase is iron carbide in an optimal particle size range. The Fe/CSX203 catalysts form small crystallites of active ε'-iron carbide during reaction. The Mössbauer results of Fig. 6 indicate that Fe^0 quickly forms carbide during reaction. Some of these iron particles are apparently too large, however, and deactivate during reaction. Thus, the activation of Fe^{2+} could involve the growth of small iron carbide particles, active for the reaction, but not for excessive coking.

Nitriding affects catalyst behavior primarily through its influence on particle size. As shown in Fig. 6, the Fe/SiO_2 (B) catalyst contains 18% of the spectral area in the Fe^0 state, which quickly forms carbide during reaction, and then can be regenerated back to its original form. After nitriding, however, 81% of the area is in the nitride form, which also immediately forms a carbide during reaction. This catalyst, when rereduced, now has 80% of the iron spectral area in the Fe^0 form and the average particle size has increased as indicated by the increased hyperfine field. These large particles account for the accelerated deactivation of the nitrided catalyst in Fig. 6.

CONCLUSIONS

Supporting iron on silica or carbon can, with certain pretreatments, create a catalyst that provides high activity and stability in forming acetonitrile. The unique aspects of the best performing catalysts are either small particle size, irreducibility beyond

Fe^{2+}, and/or lack of excessive carbon deposition, all of which are interrelated. Prenitriding a silica-supported catalyst, as compared to simple prereduction, changes activity behavior, causing high initial activity, followed by decay. Mössbauer and mass spectrometry results indicate, however, that little or no nitrogen remains in the bulk after the first few minutes on stream. Thus, changes in kinetic behavior are best accounted for by the increase in particle size that accompanies nitriding. The iron on carbon catalyst is unusually stable for the reaction, after either prenitriding or prereduction, and has the characteristic of extremely small particle size, as evidenced by the existence of superparamagnetic iron and high hydrogen uptake values. These results suggest that iron carbide is the active phase, and that smaller particles are more stable for the reaction.

ACKNOWLEDGMENTS

We are grateful for support of this work by the National Science Foundation (Grant CBT 8519688) and the Exxon Education Foundation. We also thank Professor N. Otsuka for obtaining the TEM images of the Fe/CSX203 catalyst.

REFERENCES

1. Ruhrchemie, German Patent DBP 904,891 (1949).
2. Brown (WRGrace), U.S. Patent 3,726,926 (1973).
3. Lapidus, A. L., Krylova, A. Yu., Petrachkova, N. E., Khlebnikova, T. V., and Hoang, T. V., *Izv. Akad. Nauk. SSSR, Ser. Khim.* **6,** 1257 (1985).
4. Olivé, G., and Olivé, S., *J. Mol. Catal.* **4,** 378 (1978).
5. Kliger, G. A., Glebov, L. S., Popova, T. P., Marchevskaya, E. V., Beryezkin, V. G., and Loktev, S. M., *J. Catal.* **111,** 418 (1988).
6. Olivé, G., and Olivé, S., U.S. Patent 4,179,462 (Dec. 19, 1979).
7. Gambell, J. W., and Auvil, S. R., U.S. Patent 4,272,451 (June 9, 1981).
8. Auvil, S. R., and Penquite, C. R., U.S. Patent 4,272,452 (June 9, 1981).
9. Hamada H., Kuwahara, Y., Matsuno, Y., and Wakabayashi, K., *Sekiyu Gakkaishi* **30,** 188 (1987).
10. Tatsumi, T., Kunitomi, S., Yoshiwara, J., Muramatsu, A., and Tominaga, H., *Catal. Lett.* **3,** 223 (1989).
11. Anderson, R. B., *Cat. Rev. Sci. Eng.* **21,** 53 (1980).
12. Hummel, A. A., Wilson, A. P., and Delgass, W. N., *J. Catal.* **113,** 236 (1988).
13. Lowell, S., "Introduction to Powder Surface Area." Wiley, New York, 1979.
14. Raupp, G. B., and Delgass, W. N., *J. Catal.* **58,** 337 (1979).
15. Chen, A. A., Vannice, M. A., and Phillips, J., *J. Phys. Chem.* **91,** 6257 (1987).
16. Amelse, J. A., Schwartz, L. H., and Butt, J. B., *J. Catal.* **72,** 95 (1981).
17. School of Materials Engineering, Purdue University.
18. Hochman, R. F. *in* "Proceedings, 4th International Congress on Metal Corrosion" (N. E. Hammer, Ed.), p 258. Nat. Assoc. Corros. Eng., Houston, Texas, 1972.
19. Howsmon, G. J., Ph.D. Thesis, Purdue University 1992.
20. Wivel, C., and Morup, S., *J. Phys. E: Sci Instrum.* **14,** 513 (1981).
21. Sommen, A. P. B., Stoop, F., and van der Wiele, K., *Appl. Catal.* **14,** 277 (1985).
22. Watanabe, M., *Appl. Catal.* **38,** 1 (1988).
23. Kieffer, E. P., and van der Baan, H. S., *Appl. Catal.* **3,** 245 (1982).
24. Boellaard, E., de Bokx, P. K., Kock, A. J. H. M., and Gue, J. W., *J. Catal.* **96,** 481 (1985).
25. McDonald, M. A., Storm, D. A., and Boudart, M., *J. Catal.* **102,** 386 (1986).
26. Jung, H-J., Walker, P. L., Jr., and Vannice, M. A., *J. Catal.* **75,** 416 (1982).
27. Venter, J., Kaminsky, M., Geoffroy, G. L., and Vannice, M. A., *J. Catal.* **105,** 155 (1987).
28. Jung, H-J., Vannice, M. A., Mulay, L. N., Stanfield, R. M., and Delgass, W. N., *J. Catal.* **76,** 208 (1982).
29. Jones, V. K., Neubauer, L. R., and Bartholomew, C. H., *J. Phys. Chem.* **90,** 4832 (1986).
30. Tau, L. M., and Bennett, C. O., *J. Phys. Chem.* **90,** 4825 (1986).
31. Kikuchi, E., Inoue, S., and Morita, Y., *Nippon Kaguku Kaishi* **2,** 185 (1982).
32. Chen, G. M., Jaggi, N. K., Butt, J. B., Yeh, E., and Schwartz, L. H., *J. Phys. Chem.* **87,** 5326 (1983).
33. Yeh, E., Jaggi, N. K., Butt, J. B., and Schwartz, L. H., *J. Catal.* **91,** 231 (1985).
34. Hobson, M. C., Jr., *Nature (London)* **214,** 79 (1967).
35. Delgass, W. N., Garten, R. L., and Boudart, M., *J. Phys. Chem.* **73,** 2970 (1969).
36. Somorjai, G. A., "Chemistry in Two Dimensions: Surfaces," Cornell Univ. Press, Ithaca, New York, 1981.
37. Niemantsverdriet, J. W., van der Kraan, A. M., and Delgass, W. N., *J. Catal.* **89,** 138 (1984).
38. Mørup, S., Dumesic, J. A., and Topsøe, H., *in* "Applications of Mössbauer Spectroscopy" (R. L., Cohen, Ed.), Vol II, p. 1. Academic Press, San Diego, 1980.

39. Mørup, S., and Topsøe, H., *Appl. Phys.* **11,** 63 (1976).
40. Mørup, S., Clausen, B. S., and Topsøe, H., *J. Phys.* **41,** C1-331 (1980).
41. Niemantsverdriet, J. W., van der Kraan, A. M., Delgass, W. N. and Vannice, M. A., *J. Phys. Chem* **89,** 67 (1985).
42. Niemantsverdriet, J. W., van der Kraan, A. M., van Dijk, W. L., and van der Baan, H. S., *J. Phys. Chem.* **84,** 3363 (1980).
43. Anderson, R. B., *in* "Catalysis" (P. H., Emmett, Ed.), Vol IV. Reinhold, New York, 1956.
44. Matsumoto, H., and Bennett, C. O., *J. Catal.* **53,** 331 (1978).
45. Bianchi, D., Tau, L. M., Borcar, S., and Bennett, C. O., *J. Catal.* **84,** 358 (1983).
46. Bianchi, D., Borcar, S., Teule-Gay, F., and Bennett, C. O., *J. Catal.* **82,** 442 (1983).
47. Tau, L. M., Borcar, S., Bianchi, D., and Bennett, C. O., *J. Catal.* **87,** 36 (1984).
48. Tau, L. M., and Bennett, C. O., *J. Catal.* **89,** 285 (1984).
49. Stewart, I., Tricker, M. J., and Cairns, J. A., *J. Catal.* **94,** 360 (1985).
50. Lankhorst, P. P., DeJongste, H. C., and Ponec, V., *in* "Catalyst Deactivation" (B. Delmon and G. P. Froment, Eds.), p. 43. Elsevier, Amsterdam, 1980.
51. Barbier, J., Corro, G., Zhang, Y., Bournonville, J. P., and Franck, J. P., *Appl. Catal.* **13,** 245 (1985).
52. Borowiecki, T., *Appl. Catal.* **4,** 223 (1982).
53. Schepers, F. J., van Broekhoven, E. H., and Ponec, V., *J. Catal.* **96,** 82 (1985).
54. van Senden, J. G., van Broekhoven, E. H., Wreesman, C. T. J., and Ponec, V., *J. Catal.* **87,** 468 (1984).
55. Froment, G. F., and Nam, I. S., *J. Catal.* **108,** 271 (1987).
56. Reymond, J. P., Pommier, B., and Teichner, S. J., *in* "Metal–Support and Metal-Additive Effects in Catalysis" (B. Imelik *et al.*, Eds.), p. 337. Elsevier, Amsterdam 1982.
57. Blanchard, F., Reymond, J. P., and Teichner, S. J., *J. Mol. Catal.* **17,** 171 (1982).
58. Reymond, J. P., Pommier, B., Mériaudeau, P., and Teichner, S. J., *Bull. Soc. Chim. Fr.* **5,** 173 (1980).
59. Reymond, J. P., Mériaudeau, P., and Teichner, S. J., *J. Catal.* **75,** 39 (1982).